A SINGLE-CHIP OSCILLATOR BASED ON A DEEP-SUBMICRON GAP CMOS-MEMS RESONATOR ARRAY WITH A HIGH-STIFFNESS DRIVING SCHEME

Huan-Chun Su[1], Ming-Huang Li[1], Chao-Yu Chen[1], and Sheng-Shian Li[1,2]*
[1]Institute of NanoEngineering and MicroSystems, [2]Department of Power Mechanical Engineering
National Tsing Hua University, Hsinchu, Taiwan

ABSTRACT

This work reports the design of a monolithic oscillator based on a low motional impedance (R_m) CMOS-MEMS resonator array with a high-stiffness driving scheme in a standard 0.35 µm CMOS. Combined with the previously developed polysilicon release process and the proposed "contact-array-assisted" transducer design, a tiny equivalent transducer's gap (d_{eff}) of only 190 nm is successfully attained. Based on this feature, a low R_m of 10 kΩ is achieved under a medium bias voltage (V_P) of 36 V for a 4.22-MHz resonator, which demonstrates the lowest R_m among its CMOS-MEMS counterparts to date. The combination of the mechanically coupled array and high-stiffness driving scheme significantly enhances oscillator performance in terms of far-from-carrier phase noise. The 4.22-MHz single-chip CMOS-MEMS oscillator exhibits the phase noise of -90 dBc/Hz at 1-kHz offset and -121 dBc/Hz at 1-MHz offset, respectively.

KEYWORDS

CMOS-MEMS, monolithic integration, oscillator, motional impedance, high-stiffness driving, phase noise.

INTRODUCTION

Oscillators are an important building block in the modern electronic systems to provide accurate and stable clock signals [1]. Temperature compensated crystal oscillator (TCXO) is a proven technology widely used in low-noise timing applications with excellent temperature stability. However, the bulky size of the TCXOs becomes a main issue against emerging applications such as wireless sensor networks (WSN) and Internet of Things (IoT). Although *LC*-tank based oscillators [2] have demonstrated low jitter and temperature stable operations without using external resonators, their significant power consumption still places a bottleneck for portable applications.

Recently, microelectromechanical systems (MEMS) based oscillators become an applicable solution because of their tiny size, low cost, high-*Q*, and integration capability with commercial CMOS processes [3-5]. In particular, the monolithic CMOS-MEMS technology offers a design platform for MEMS oscillator applications [6]. For example, the oven-controlled monolithic CMOS-MEMS oscillator has recently been demonstrated with a figure-of-merit (FoM) of -172 dB at 1-kHz offset under power consumption less than 2 mW for temperature stable operations [6]. However, the performance of the MEMS resonators fabricated by CMOS technology is substantially limited by the material properties and the technological design rules in CMOS. Traditional capacitive CMOS-MEMS resonators often exhibit high motional impedance in a range of 0.1 to 10 MΩ owing to their large gap spacing and insufficient transduction areas [6]. Such high R_m not only makes the oscillator design very difficult, but also introduces additional thermal-mechanical noise in the oscillation spectrum [6].

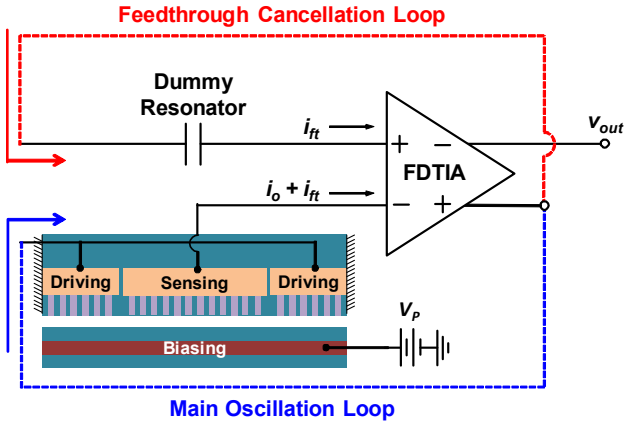

Figure 1: Circuit schematic of the monolithic CMOS-MEMS oscillator with a feedthrough cancellation scheme.

To solve the abovementioned issues, the purpose of this work is to realize a monolithic CMOS-MEMS oscillator based on a low motional impedance (R_m) resonator array. The advanced two-step polysilicon release process [4] with the newly proposed "contact-array-assisted" gap spacing design are the keys for achieving low R_m in a 0.35 µm CMOS platform. The high-stiffness driving scheme [7] is adopted to further improve the power handling capability of the resonant tank. The monolithic oscillator designed in this work shows a far-from-carrier phase noise of -121 dBc/Hz with a 4.22 MHz carrier frequency.

RESONATOR & OSCILLATOR DESIGN

Overall Architecture

The schematic of the oscillator circuit presented in this work is depicted in Fig. 1, which is a series resonant circuit topology composed of two identical MEMS resonators and a fully-differential transimpedance amplifier (FD-TIA). To suppress the possible capacitive feedthrough signal often observed in high frequency CMOS-MEMS resonators [4], an active feedthrough cancellation scheme is utilized in this work. As depicted in Fig. 1, one of the resonators is connected in the main oscillation loop to generate a desired resonant signal at the designed resonance frequency, while the other one (i.e., the dummy resonator) is connected in the

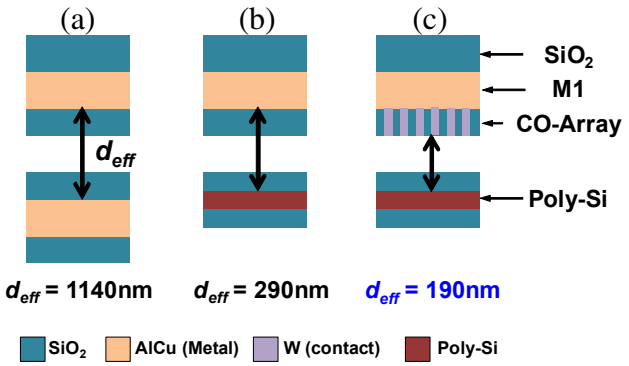

Figure 2: Cross-sectional view showing various transduction gap configurations of (a) metal-to-metal, (b) metal-to-polysilicon, and (c) metal-to-polysilicon with contact-array.

feedthrough cancellation loop to eliminate the common mode feedthrough currents, i_{ft}. With such a feedthrough cancellation configuration, a 10-dB off-resonance rejection is observed for the proposed resonator in its open-loop measurements.

Low Impedance Resonator Design

The resonator is the fundamental element of an oscillator, which provides function of frequency selection. In this work, the clamped-clamped beam resonator is adopted to generate 4.22-MHz resonant signal under a medium bias voltage of 36 V thanks to its simple and robust mechanical structure. To access a tiny transduction gap and decrease R_m of the resonator in a standard 0.35 µm CMOS process, the metal and polysilicon wet etching processes have been developed [4], where a satisfactory capacitive transduction can be attained either using metal-to-metal gap (cf. Fig. 2(a)) or metal-to-polysilicon gap (cf. Fig. 2(b)). However, these configurations are still insufficient for attaining R_m of sub-10 kΩ in a two-port resonator. In this work, a novel "contact-array-assisted" design is proposed to further reduce R_m by *inserting an array of tungsten contacts* between metal and polysilicon electrodes (cf. Fig. 2(c)), which leads to an equivalent gap of only 190 nm.

In addition to the motional impedance, the power handling capability of the MEMS resonator also plays an important role in the phase noise performance of the implemented oscillator. Typically, the *linear* resonator operation in the oscillation loop is preferred for attaining low phase noise. However, the use of a tiny gap will dramatically reduce the power handling capability of the resonator and induce nonlinear effects as operated in a nonlinear region [1]. To address the nonlinearity issue for the narrow-gap resonators, the high-stiffness driving scheme [7] is used in the presented resonator. Fig. 1 also shows the schematic of the cross-sectional view of a designed two-port clamped-clamped beam resonator with a high-stiffness driving scheme. The biasing electrode (polysilicon layer) is placed underneath the clamped-clamped beam structure to serve as a common biasing plane with a voltage potential V_P. The driving and sensing metal electrodes are embedded

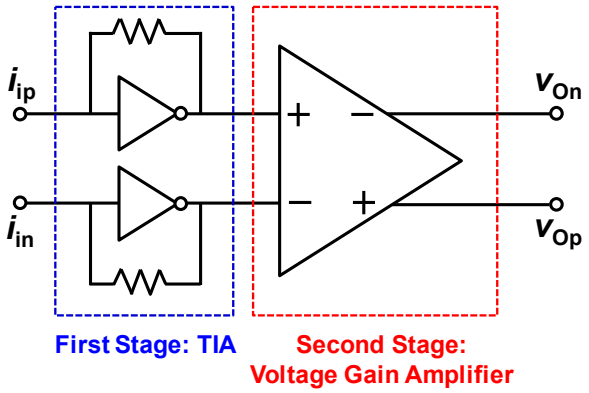

Figure 3: Top-level circuit schematic of the FD-TIA.

inside the resonator structure. Note that the driving electrode is separated into two pieces located at two ends of the clamped-clamped beam for high-stiffness driving operations, while the sensing electrode is placed at the central low-stiffness region. By using the high-stiffness driving scheme, the power handling capability of the resonator could be greatly improved [7].

To further reduce the motional impedance and improve the power handling capability of the resonator, the resonator array concept [8] is also implemented. The designed resonant tank is formed by multiple (five) high-velocity coupled clamped-clamped beams to gain large transduction area and high effective stiffness, thus enhancing power handling capability and reducing motional impedance of the resonator.

CMOS FD-TIA Circuit Design

One design challenge of a MEMS oscillator circuit is to build up a sustaining amplifier with high transimpedance gain and sufficient bandwidth to compensate the loss of the MEMS resonator. Thanks to the low-R_m design proposed in this work, moderate transimpedance gain (e.g., 10-100kΩ) is more than sufficient to meet oscillation. Together with the active and dummy MEMS units aforementioned, a fully-differential circuit topology is used to enable feedthrough cancellation. Fig. 3 shows the top-level circuit scheme of the FD-TIA which consists of two stages. The first stage is an inverter-based shunt-shunt feedback TIA to convert the motional current into voltage signal. The second stage is a high-bandwidth, moderate voltage amplifier, which is designed based on a Cherry-Hooper configuration.

FABRICATION

To create a deep-submicron transduction gap to lower the motional impedance of the resonator, the previously developed maskless metal etching post-process combined with a polysilicon etching technique is used. The contact-array-assisted design proposed in this work will not affect the post-CMOS process.

The chip was fabricated by a TSMC 0.35 µm 2P4M standard CMOS process as shown in Fig. 4(a) where the circuit region is covered by a passivation layer to protect it from damage during the post-process. First, the metal wet

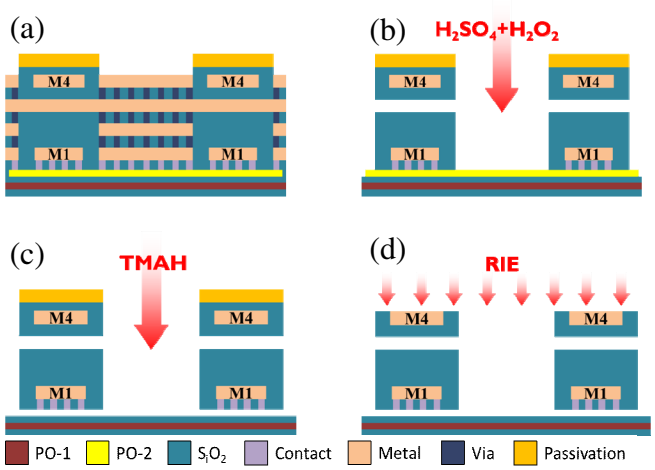

Figure 4: MEMS post-process of (a) after standard 0.35 µm CMOS, (b) metal wet etching, (c) polysilicon wet etching, and (d) RIE.

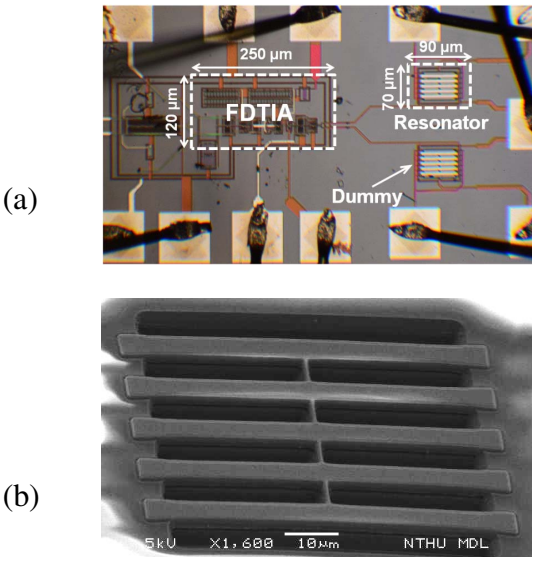

Figure 5: (a) Optical photo of the monolithic CMOS-MEMS oscillator. (b) SEM of the clamped-clamped beam resonator array.

etching solution composed of H_2SO_4 and H_2O_2 was utilized to remove the sacrificial layers including aluminum and tungsten vias, thus defining the resonator structure as shown in Fig. 4(b). In order to release the beam structure, the 25% TMAH solution was used to etch the polysilicon layer (PO2) and then a 190-nm transduction gap was achieved as shown in Fig. 4(c). Finally, in Fig. 4(d), we used RIE to etch the passivation layer above the pads and open the pads for later wire-bonding. Also note that the top metal layer (Metal-4) serves as a hard mask to protect the resonator structure during the RIE process. Fig. 5(a) presents the global-view optical photo of the monolithic oscillator including the micro resonator and FD-TIA circuit after the post-process. Fig. 5(b) shows the SEM of the fabricated clamped-clamped beam resonator array and proves that the developed post-process is suitable for our proposed resonator designs.

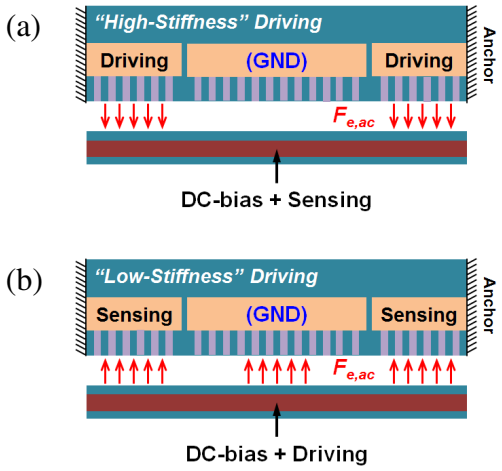

Figure 6: Schematics of (a) high-stiffness driving and (b) low-stiffness driving schemes implemented in the proposed resonator array. $F_{e,ac}$ and arrows denote the locations of the ac electrostatic driving force.

MEASUREMENT RESULTS & DISCUSSION

Open-loop Resonator Characterization

To investigate the effectiveness of the high-stiffness driving scheme for the proposed resonator, two different one-port driving configurations based on *high-stiffness driving* (cf. Fig. 6(a)) and *low-stiffness driving* (cf. Fig. 6(b)) schemes are compared. Since the center electrode is already connected with the CMOS amplifier, the electrical potential of this node is kept grounded during this measurement. Fig. 7(a) and (b) show the measured resonance spectra under high- and low-stiffness driving schemes, respectively. For high-stiffness driving, the resonator shows Q of 1,000 and R_m of 10 kΩ for linear operation, and the Duffing nonlinear behavior can be observed as the driving power (P_i) exceeds -20 dBm. In contrast, the nonlinear resonator operation of the low-stiffness driving scheme occurs at P_i of -30 dBm. Evidently, high-stiffness driving promises better power handling capability that can tolerate higher excitation power for oscillator operation. Moreover, the resonant peak in Fig. 7(b) shows a "plateau" region as P_i exceeds -15 dBm, which possibly comes from the physical contact of the MEMS resonator with its bottom electrode [9]. This phenomenon is likely caused by the large displacement of the clamped-clamped beam due to its low-stiffness driving and tiny gap between the beam structure and bottom electrode.

Monolithic MEMS Oscillator Characterization

The closed-loop schematic of the monolithic oscillator based on the proposed CMOS-MEMS resonator in a two-port configuration can be referred to Fig. 1. The dc-bias voltage (V_P) is applied on the bottom electrode to serve as a common biasing plane. The dummy resonator and fully-differential TIA are employed for active feedthrough cancellation. The MEMS resonator is connected to the negative output terminal of the fully-differential TIA to compensate the 180° phase shift of the resonator to ensure oscillation. The measured

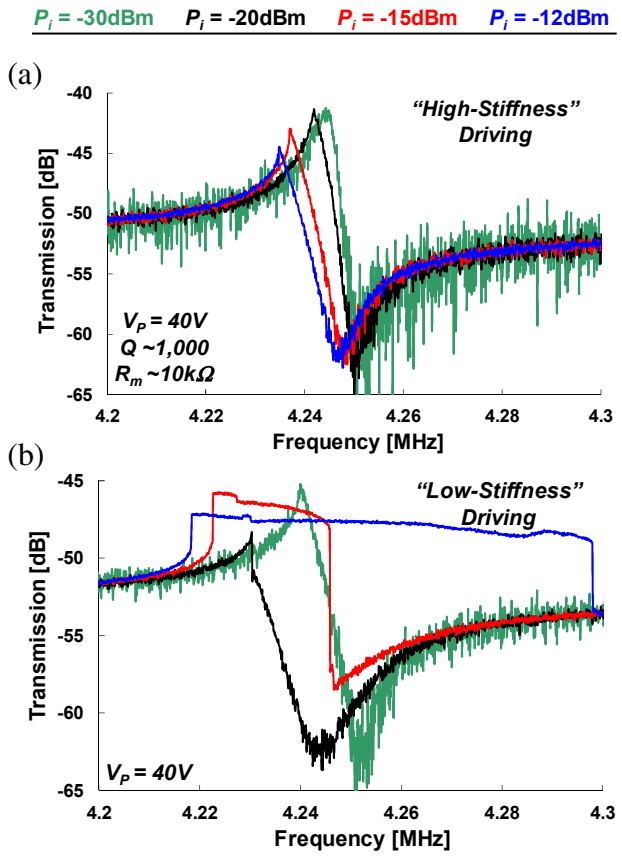

Figure 7: Measured transmission spectra of (a) high-stiffness driving and (b) low-stiffness driving schemes that correspond to Fig. 6(a) and (b), respectively.

phase noise performance of the oscillator is shown in Fig. 8 as well as the time-domain waveform in the inset. The oscillation frequency (f_o) was measured at 4.22 MHz under a medium-V_P of 36 V with a peak-to-peak amplitude of 436 mV. The lowest V_P required for oscillation is 25 V. The measured best-case phase noise is -90 dBc/Hz at 1-kHz offset and -121 dBc/Hz at 1-MHz offset, respectively, under V_P of 36 V. Thanks to the low-R_m resonator array design in this work, the far-from-carrier phase noise is better than the prior art [10] by 4 dB as scaled to the same carrier frequency.

CONCLUSION

This work demonstrates a monolithic oscillator based on a 190 nm-gap CMOS-MEMS resonator technology with the proposed "contact-array-assisted" design. To further reduce the motional impedance and improve the power handling capability of the resonator, the resonator array technique and the high-stiffness driving scheme are also adopted. The experimental results show that high-stiffness driving promises better power handling capability of the resonator, exhibiting Q of 1,000 and R_m of 10 kΩ for the linear operation. Also, the 4.22-MHz oscillation signal was measured with a medium-V_P of 36 V, and the measured phase noise is -90 dBc/Hz at 1-kHz offset and -121 dBc/Hz at 1-MHz offset, respectively.

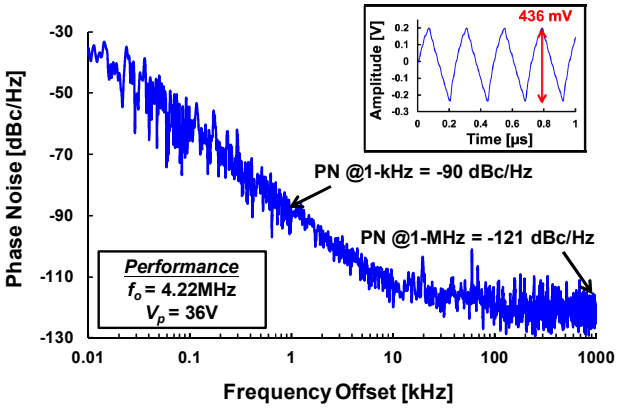

Figure 8: Measured phase noise performance of the oscillator based on the proposed CMOS-MEMS resonator array.

ACKNOWLEDGEMENTS

The authors would like to appreciate the TSMC and the Chip Implementation Center (CIC), Taiwan, for their support of IC manufacturing. The authors also appreciate the Center of Nanotechnology, Materials Science and Microsystems of National Tsing Hua University for the use of fabrication facilities.

REFERENCES

[1] J. van Beek and R. Puers, "A review of MEMS oscillators for frequency reference and timing applications," J. Micromech. Microeng., vol. 22, no. 1, pp. 013001, Jan. 2012.

[2] M. McCorquodale *et al.*, "A monolithic and self-referenced RF LC clock …," *IEEE J. Solid-State Circuits*, vol. 42, no. 2, pp. 385-399, Feb. 2007.

[3] S.-S. Li, "CMOS-MEMS resonators and their applications," *Proc. UFFC'13*, pp.915-921, July 2013.

[4] C.-Y. Chen, *et al.*, "Design and characterization of mechanically coupled CMOS-MEMS filters …," *Sens. Actu. A: Phys.*, vol. 216, Sep. 2014, pp. 394- 404.

[5] M.-H. Li *et al.*, "Design and characterization of a dual-mode CMOS-MEMS resonator …," *J. Microelectromech. Syst.*, to be published.

[6] M.-H. Li *et al.*, "A monolithic CMOS-MEMS oscillator based on an ultra-low-power ovenized micromechanical resonator," *J. Microelectromech. Syst.*, to be published.

[7] L.-J. Hou and S.-S. Li, "High-stiffness driven micromechanical resonators …," *Appl. Phys. Lett.*, vol. 100, no. 13, pp. 131908, 2012.

[8] M. U. Demirci and C. T.-C. Nguyen, "Mechanically corner-coupled …," *J. Microelectromech. Systems*, vol. 15, no. 6, pp. 1419-1436, Dec. 2006.

[9] Y. Lin, et al., "A resonance dynamical …," *Proc., IEEE IFCS 2008*, pp. 640-645, May. 2008.

[10] J. Verd, et al., "A 3V CMOS-MEMS …," *Tech. Dig. Transducers 2013*, pp. 806-809, June 2013.

CONTACT

*S.-S. Li, Tel: +886-3-516-2401; ssli@mx.nthu.edu.tw